https://doi.org/10.5194/egusphere-2025-1171
Preprint. Discussion started: 19 March 2025

A new method to retrieve relative humidity profiles from a synergy of Raman lidar, microwave radiometer and satellite

Chengli Ji[1], Qiankai Jin[2], Feilong Li[2], Yuyang Liu[2], Zhicheng Wang[1], Jiajia Mao[1], Xiaoyu Ren[1], Yan Xiang[4], Wanlin Jian[5,6], Peitao Zhao*[1], and Zhenyi Chen*[2,3]

[1] CMA Meteorological Observation Centre, Beijing, 100081, China

[2] State Environmental Protection Key Laboratory of Food Chain Pollution Control, Beijing Technology and Business University, Beijing, 100048, China

[3] Key Lab. of Environmental Optics & Technology, Anhui Institute of Optics and Fine Mechanics, Chinese Academy of Sciences, Hefei, 230031, China

[4] Institutes of Physical Science and Information Technology, Anhui University, Hefei, 230031, China

[5] Sichuan Meteorological Observation and Data Center, Chengdu, 610072,China

[6] Sichuan Meteorological Observatory Heavy rain and Drought－Floor Disaster in Plateau and Basin Key Laboratory of Sichuan Province,Chengdu, 610072,China

**Corresponding author*: E－mail: zychen@btbu.edu.cn (Zhenyi Chen), peitaozhao@163.com (Peitao Zhao)

Abstract Precise continuous measurements of relative humidity (RH) vertical profiles in the troposphere have emerged as a considerable scientific issue. In recent years, a combination of diverse ground-based remote sensing devices has effectively facilitated RH vertical profiling, leading to enhancements in spatial resolution and, in certain instances, measurement accuracy. This work introduces a newly developed approach for obtaining continuous RH profiles by integrating data from a Raman lidar, a microwave radiometer, and satellite sources. RH profiles obtained using synergistic approaches are subsequently compared with radiosonde data throughout a five-month observational study in China. Our suggested method for RH profiling demonstrates optimal concordance with the best correction coefficients R of 0.90 in Huhehaote

https://doi.org/10.5194/egusphere-2025-1171
Preprint. Discussion started: 19 March 2025

(HHHT), 0.91 in Yibin (YB) and 0.93 in Qingyuan (QY), respectively. Accordingly, the mean bias (MB) reached the lowest values of 4.93% in HHHT, 2.63% in YB and 2.40% in QY. The mean value of RH decreased with height and presented seasonal characteristics in QY. Finally, the RH height-time evolution in a convective case was analyzed. This study firstly integrates satellite data into ground-based measurement to provide information on RH profiles in China, which may aid in further evaluating their regional characteristic and their impacts on the local ecosystem.

Keywords: relative humidity profiles, Raman lidar, microwave radiometer, satellite

1. Introduction

Relative humidity (RH) is a crucial parameter in characterizing aerosol-cloud interactions (Fan et al., 2007) and is necessary as input for weather forecasting models (Petters and Kreidenweis, 2007; Wex et al., 2008; Mochida, 2014). The combination of these RH profiles with aerosol optical data allows us to obtain hygroscopic growth factors for different aerosol types (Zieger et al., 2013; Granados et al., 2015). However, the temporal resolution of routine observations performed by weather services is rather low, typically with one or two radiosonde launches per day (Schmetz et al., 2021). And significant mesoscale weather phenomena, including the movement of frontal systems and the formation of convective boundary hygroscopic growth or clouds, transpire rapidly, making it more challenging to adequately monitor the evolution of atmospheric profiles (Kang et al., 2019; Long et al., 2023; Chen et al., 2024). Consequently, precise information with great temporal resolution is essential for examining these events.

The current Raman lidar technology enables concurrent measurements of temperature and water vapor mixing ratio profiles to derive RH profiles (Reichardt et al., 2012; Brocard et al., 2013). But it requires calibration by the use of collocated and simultaneous observations from a radiosonde or microwave radiometer (MWR) (Mattis et al., 2002; Madonna et al., 2011; Foth et al., 2015). In addition, the average error of Raman lidar is relatively small within the effective height range but limited in the higher height detection.

MVR is another way to provide atmospheric RH observations with high temporal resolution (Hogg et al., 1983; Ware et al., 2003; Zhang et al., 2024). Although MVR has a certain penetration ability for harsh weather conditions such as clouds, their vertical resolution and accuracy are not high, especially for RH which vary greatly (Xu et al., 2015). For accurate RH profile retrieval at higher heights, space-borne MVR have global detection capabilities and are highly effective for oceanic skies and remote land areas (Zhang et al., 2022; Wang et al., 2023). But the time resolution of polar orbit satellites equipped with MVR is determined by the

https://doi.org/10.5194/egusphere-2025-1171
Preprint. Discussion started: 19 March 2025

repeated coverage time of the satellite orbit (Skou, et al., 2022). A single satellite can generally only achieve repeated observations twice a day, and the time resolution is also relatively low.

As previously indicated, it is challenging to deliver continuous high-resolution RH information with a single instrument. The synergy of complementary information from both active and passive instruments can provide a more comprehensive understanding of atmospheric processes (Stankov, 1995; Furumoto et al., 2003; Delanoë and Hogan, 2008; Blumberg et al., 2015; Tuner et al., 2021). For example, when both Raman lidar and MWR are measuring collocated and simultaneously, continuous temperature, water vapor profiles and thus RH profiles can be obtained operationally (Navas-Guzmán et al., 2014; Barrera-Verdejo et al., 2016; Foth et al., 2017; Toporov et al., 2020).

Furthermore, at the time of the study, few observations are available from China's satellite Fenyun (FY), to the use of synthetic retrieval of RH information. This study aims to introduce a novel technique that integrates Raman lidar, MWR, and satellite data (FY4B) using an optimum estimating methodology. It is given with a focus on two aspects: i) Evaluation of the proposed synergetic method, and ii), investigation of the RH characteristics at different heights and in different geographic regions. This paper is thus structured as follows. Descriptions of the individual equipment is presented in Section 2. Section 3 illustrates the process of the new synergetic algorithm combining the ground-based and satellite data. Section 4 presents the RH statistic results and its time-height evolution in a strong convective case. Finally, conclusions are summarized in Section 5.

2. Instrumentation

2.1 Raman lidar

The Raman lidar method can assess the water vapor mixing ratio profiles through inelastic backscattering signals from nitrogen at 387 nm and from water vapor at 407 nm (Whiteman, 1992; Mattis et al., 2002; Adam et al., 2010). At the lowest height, the intersection of the laser beam with the receiver's field of view in the bistatic system is incomplete. Nevertheless, the overlap of both Raman channels is presumed to be equivalent; thus, the overlap effect could be minimal concerning water vapor measurements. But the signal-to-noise ratio (SNR) decreases with height, thus the threshold of SNR should be set. Here we set the Raman SNR threshold value of 3. The Raman signal starts with the first SNR greater than 3 and ends with five consecutive SNRs less than 3. The collected water vapor measurements, then along with concurrent temperature profiles from a co-located MVR allow us to obtain RH profiles. The vertical and temporal resolution of Raman lidar and other instruments are listed in Table 1.

2.2 Microwave Radiometer (MVR)

The Microwave Radiometer (MVR) serves as a passive instrument designed to measure atmospheric emissions across two frequency bands within the microwave spectrum (Cimini et al., 2006; Crewell and Löhnert, 2007). There are seven channels set along the 22.235 GHz H_2O absorption line. Humidity information can be extracted from these observations. The seven channels of the alternative band from 51 to 58 GHz within the O_2 absorption complex encompass the vertical temperature profile data. Consequently, the fully automatic MVR enables the derivation of temperature and humidity profiles with a temporal resolution of up to 5 minutes. The method for inverting temperature and humidity profiles is the neural network method in this study. It uses statistical methods to optimize the long-term average radiosonde data and relies on previous radiosonde data (Yang et al., 2023).

2.3 Radiosonde data

We use radiosonde data from the China Meteorological Administration (CMA) station for reference analysis. It is located in the same place as the Raman lidar, and provides on-site measurements of atmospheric pressure, temperature, and RH. During the observing campaign, radiosondes were launched twice a day (08:00 LST and 20:00 LST). The height of the radiosonde balloon can be determined by the ascent time of the radiosonde balloon. The uncertainty of the instrument can reach a confidence level of 95.5%. The vertical resolution of the raw data is 3 m/layer. To match other data, the vertical resolution of the raw data is interpolated to 30 m (0-3000 m) and 250 m (3000-10000 m), respectively.

2.3 Satellite

In 2016 and 2021, China successfully deployed two second-generation geostationary meteorological satellites, Fengyun-4A (FY4A) and Fengyun-4B (FY4B), both equipped with the Geostationary Interferometric Infrared Sounder (GIIRS). The GIIRS therefore became the first geostationary orbiting meteorological satellite (Yang et al., 2023). This approach could achieve the detection of weather systems across China and its neighboring regions with high temporal and spatial resolution. So it enables a more comprehensive understanding of the atmospheric vertical structure, including the retrieval of atmospheric temperature profiles for 1000 m layers and moisture profiles for 2000 m layers (Yang et al., 2017), respectively. In comparison to FY4A, the GIIRS on FY4B exhibits a broader spectral range, improved spectral resolution in the long-wave IR band, and superior radiometric calibration accuracy and detection sensitivity (Sufeng et al., 2022). Specifically, the temporal resolution of GIIRS has enhanced from 2.5 hours for FY4A to 2 hours for FY4B, and the spatial resolution has progressed from 16000 m to 12000 m at nadir. The atmospheric humidity profiles utilized in

https://doi.org/10.5194/egusphere-2025-1171
Preprint. Discussion started: 19 March 2025

this study, derived from GIIRS, are generated through the neural network algorithm created by the National Satellite Meteorological Centre (NSMC) (Bai et al., 2022). The data is available online: http://fy4.nsmc.org.cn/nsmc/en/ theme/FY4B.html (accessed on 12 December 2024).

3. Methods and evaluation

3.1 Lidar, MVR and satellite synergetic algorithm

This study aims to obtain a continuous time series of RH profiles by integrating ground-based remote sensing techniques, including Raman lidar, MVR, and satellite data, in a straightforward manner to facilitate a wide range of applications. The retrieval process involves a systematic four-step algorithm that integrates the Raman lidar water mixing ratio profile and MWR brightness temperatures along with satellite data. The retrieval framework is shown as in Fig. 1 and the retrieval process is detailed in the following paragraphs.

Step 1: Data quality control. Data with quality control codes of 0 and 1 for FY4B and 0 for ground-based remote sensing data is selected. The Ramna lidar only retains data with a SNR value greater than 3. Then the triple standard deviation method is utilized to eliminate anomalies. The real-time observing data are designated as R_{radio}, R_{lidar} , R_{MVR} and $R_{satellite}$ in Fig. 2.

Step 2: Data spatial-temporal matching. This process aims to match the above quality-controlled data with the radiosonde data at a height of 0-10000 m in time and space before the synergetic algorithm. For the time matching, temperature from MVR and water vapor data from Raman lidar are selected corresponding to the radiosonde data time (00:80 LST and 20:00 LST). In terms of spatial matching, the FY4B data is selected from the nearest grid point to the ground observing station for the horizontal scale. The data at vertical heights are interpolated to the resolution of 30 m (0-3000 m) and 250 m (3000-10000 m).

Step 3: Correction coefficient determination. The deviation between the temperature and humidity data of satellites and ground-based remote sensing data at each height is quantitatively calculated and analyzed to prepare for the optimal stitching process in the next step. Here the deviation of each instrument is designated as $D_{lidar,}$ D_{MVR} and $D_{satellite}$, respectively. The calculation of correction coefficients $C_{lidar,}$ C_{MVR} and $C_{satellite}$ are also presented in Fig. 2.

Step 4: Synergetic algorithm iteration and evaluation: Based on the above spatial-temporal data matching and correction coefficients calculation at different heights, a dynamic optimal stitching algorithm (Fig. 2) is conducted. To ensure the independence between the tested sample and the true value, the temperature and humidity profiles of the current time are fused using the correction coefficient of the previous time, and then compared with the radiosonde

https://doi.org/10.5194/egusphere-2025-1171
Preprint. Discussion started: 19 March 2025

data at the same time for evaluation. The correlation coefficient (R), the root mean square error (RMSE), and mean bias (MB) are used as inspection indexes. Finally, the retrieved RH information S_{RH} could be obtained.

3.2 Error analysis

To evaluate the performance of the synergetic algorithm for RH profiles, a comparative analysis was conducted between retrieved values and actual radiosonde measurements. Let N represent the total number of samples. The measured value is designated as Oi, with i representing the sample label. The value obtained through the new synergetic algorithm is designated as Gi. The evaluation indicators consist of MB, mean absolute bias (MAB) and RMSE are defined by the following formulas:

$$MB = \frac{\sum_{i=1}^{N}(G_i - O_i)}{N} \tag{1}$$

$$MAB = \frac{\sum_{i=1}^{N}|G_i - O_i|}{N} \tag{2}$$

$$RMSE = \sqrt{\frac{\sum_{i=1}^{N}(G_i - O_i)^2}{N}} \tag{3}$$

4. Results

4.1 General statistic information

A five-month data set has been chosen for a statistical analysis of RH profiles. The observation period spans from July 1 to November 30, 2024. The observing elements are RH data from 47 stations in China (yellow circles in Fig. 3) at the height of 0-10000 m. To investigate RH retrieval accuracy, we provide the comparison results of four methods (lidar, MVR, satellite, and synergetic algorithm) utilizing the radiosonde data as the reference at 47 sites in Table 2. Then Huhehaote (HHHT, northern China), Yibin (YB, middle China) and Qingyuan (QY, southern China) are selected as 3 representative sites (red stars in Fig. 3) for more detailed analysis, as shown in Fig. 4 and Table 3.

Generally, the synergetic algorithm at 47 sites presents the maximum correlation coefficient R value of 0.98 with the minimum RMSE of 5.27% in Table 2. For three representative sites, the regression line from the synergetic algorithm at all heights similarly provides the best fitting results, with the largest correlation coefficients R of 0.90, 0.91 and 0.93 in HHHT, YB and QY respectively (Table 3). The correlation coefficient R for lidar measurement follows with

https://doi.org/10.5194/egusphere-2025-1171
Preprint. Discussion started: 19 March 2025

marginally lower values of 0.85 in HHHT, 0.85 in YB and 0.91 in QY, indicating its greater applicability compared to other single instruments. MVR presents the lowest R of 0.73 and 0.80 in HHHT and YB, while performing better (R = 0.84) than that from satellite (R = 0.78) in QY. In terms of RMSE, the lidar-, MVR- and satellite-derived RH all show values larger than 25% at three sites. The synergistic use of a multi-source algorithm decreases the RMSE down to the lowest value of 16% in QY.

The regression line for lidar and MVR in HHHT, as illustrated in Fig. 4, exhibits a slope that is less than that of the one-to-one line. This implies that greater variations arise with increased RH in HHHT. Though the synergetic algorithm also presents similar trends, its RMSE decreased to 26% in HHHT. The regression line of MVR and lidar in YB and QY are larger than the one-to-one line, indicating the larger bias for less humid.

As RH vertical profiles are height-dependent, Fig. 5 presents the MB profiles observed at different heights in terms of four methods. Generally, the MB in the RH of lidar in the lower troposphere (below 3000 m) outperforms the other two single methods (MVR and satellite) at three sites. No significant biases between radiosonde and lidar are noticeable. Specifically, the lowest MB values (4.93% in HHHT, 2.63% in YB and 2.40% in QY) in the comprehensive region of the tropospheric region are achieved when lidar data is incorporated into the synergetic algorithm. This is because lidar is an active remote sensing technology with more accuracy compared to MVR and satellite. The lidar data's efficacy is enhanced at heights below 3000 m when integrated with data from other sources within the boundary layer.

However, the MB from lidar increased drastically above this height, up to the highest value 28.67% in HHHT, 29.91% in YB and 20.09 % in QY. It is reasonable that the atmosphere changes so fast that radiosonde do not assess exactly the same air mass as lidar. In the meantime, lidar is increasingly constrained at elevated heights because of a decreased SNR. Hence lidar is more trustworthy in the lower layer, i.e. below 3000 m.

In contrast, the MB from satellite (FY4B) over 3000 m varied steadily within the range of approximately 15% at three sites. Therefore the satellite data in the far height range would be more reliable and could be employed in the synergetic algorithm at higher layers. Compared to lidar and satellite, the MB from MVR gives the largest uncertainty in HHHT at all heights. This may result from the discrepancy between the temperature recorded by the radiosonde and that obtained from the MVR in HHHT. However, it yields relatively less variation than lidar and satellite in YB and QY. Anyway, the synergetic method gives the best result for over three observing sites at almost all heights. And accurate measurements of RH vertical profiles provided here are highly beneficial for analyzing the hygroscopic growth of local aerosols.

https://doi.org/10.5194/egusphere-2025-1171
Preprint. Discussion started: 19 March 2025

The sources of the discrepancy can stem from several aspects. First, although all instruments are co-located in the ground, radiosondes deviate at higher heights, and signals can be disrupted if clouds are present. Second, satellites provide gridded data, requiring the selection of ground observation points closest to its grid's latitude and longitude, which introduces uncertainty. Finally, both MVR and satellite are passive remote sensing technologies, which are inherently less precise than active remote sensing. Besides the inherent hardware difference, the errors during the retrieval process (e.g., neural networks for MVR) are also unavoidable.

4.2 Mean monthly analysis

RH mean monthly vertical profiles have been derived from the synergistic method illustrated in Fig. 6. Because RH profiles were retrieved from water ratio profiles and temperature profiles. For this property, the RH seasonal behavior may be more complicated. For example, no obvious seasonal behavior of RH profiles is found in HHHT or YB. However, QY still presents the most likely seasonal characteristic at most of the heights, with the highest mean values in summer at 1000-2000 m (80.65% in July) and lowest values at 7000-10000 m in late autumn (20.50% in November) in Fig. 6e-f. The elevated RH observed in QY's summer may be related to the sufficient water vapor and large transport volume as QY is located in coastal areas. So the characteristic of QY would be more dependent on water vapor.

For comparison, HHHT and YB are relatively random. Over 3000 m in HHHT (Fig. 6a-b), RH in August shows predominantly high values with the highest value of 65.37% at 5000-7000 m. Different from HHHT and QY, the RH profiles in November of YB interestingly show the highest values (83.95%) in the lower atmosphere (0-1000 m) in Fig. 6c-d. It suggests the reduced temperatures observed in autumn of YB promote proximity to saturation conditions, resulting in elevated RH values in November. It is also worth noting that RH above 3000 m in November of YB decreases dramatically as height increases, with the minimum RH of 13.91% at 7000-10000 m. That could be explained by more rapid fluctuations in the water vapor density and temperature in YB in the higher layer under the control of the subtropical monsoon climate zone. Anyway, this plot illustrates a clear decrease in the RH values with heights at three sites.

4.3 Case analysis

From 19 to 20 August 2024, due to the continuous southwest warm and humid airflow around the periphery of the subtropical high and the frequent southward weak cold air from the north, large-scale heavy precipitation weather has occurred in Inner Mongolia, Northern, and Central China, and other areas. This precipitation process lasts for a long time, with rainfall and

https://doi.org/10.5194/egusphere-2025-1171
Preprint. Discussion started: 19 March 2025

accumulated high moisture. Therefore, this period was chosen for studying the RH temporal-spatial evolution.

Fig. 7 shows the ERA5-based 500 hPa (approximately 5500 m) geopotential height field, 850 hPa (approximately 1500 m) wind field, and total column precipitable water. From the night of the 19th to the morning of the 20th (LST), a stable large-scale circulation pattern formed under the combined influence of the western edge of the subtropical high and the cold vortex system over Inner Mongolia. Central Inner Mongolia and northeastern Hebei, located under the control of these two systems, experienced mid-to-upper-level airflow. HHHT was situated on the northeastern side of a low-level vortex (Fig. 7), where the convergence and shear between northeasterly and southeasterly winds provided favorable dynamic uplift conditions for precipitation. YB and QY were both located on the periphery of the subtropical high-pressure system, leading to intensified convective activity. Thus the total column water vapor content in YB and QY reached 50-60 and 60-70 mm, respectively, indicating ample moisture supply.

Accordingly, Fig. 8 shows the height-time display of RH from the synergetic retrieval during the same period at the three sites. From surface to 10000 m, RH in QY was generally higher (ranged from 60% to 90%) than that in HHHT and YB (both ranged from 10% to 80%). For vertical variation, RH decreased as the height increased in HHHT on 19 August (Fig. 8a). YB's RH experienced more spatial fluctuation at 3000-6000 m while QY's RH presented higher values through all the heights on that day. During the passage of the cold front, the warmer and more humid air originally affecting southern China was made to lift, resulting in lifted RH of 90% from 3000-6000 m in QY. Besides the cold front, QY's terrain, higher in the west and lower in the east, lies on the windward slope of low-level southeasterly airflow, further enhancing moisture convergence and uplift. Consequently, the stable circulation pattern and abundant moisture created conditions conducive to high RH in the QY region.

5. Conclusion

This study presents relative humidity (RH) measurements with a developed synergetic algorithm with the combination of Raman lidar, MVR, and satellite at three sites (northern China, middle of China and southern China) from 1 July to 31 November. First, the methodology for obtaining RH from the synergetic algorithm was introduced. A five-month field campaign was performed and linear regression between the lidar, MVR, satellite, synergetic algorithm and radiosonde data at the range 0-10000 m was presented to testify the accuracy.

Strong correlations of RH values over 0.9 were observed between radiosonde measurements and profiles derived from the synergetic approach at three representative sites in China. The

https://doi.org/10.5194/egusphere-2025-1171
Preprint. Discussion started: 19 March 2025

lowest MB values (4.93% in HHHT, 2.63% in YB and 2.40% in QY) are observed when lidar data is integrated into the synergetic algorithm, which highlights the accuracy of the lidar data below 3000 m. However, the MB from lidar increased drastically above this height, which suggests the greater applicability of satellite or MVR in the middle and higher layers. Thus, the new synergetic algorithm integrated the best-performing data from various sources with the correction coefficient, which is updated in real-time based on the latest radiosonde data. And that leads to the strong regional applicability of the algorithm.

No discernible seasonal characteristic in RH profiles are observed in HHHT or YB. Nonetheless, QY exhibits the predominant seasonal feature throughout most heights, with peak mean values of 80.65% in July at 1000-2000 m and minimal values of 20.50% in November at 7000-10000 m. Diverse atmospheric circulation patterns and geographical environments have resulted in regional variations in RH monthly mean values.

These results validate the capabilities of the newly developed method to deliver accurate measurements of RH information throughout the troposphere. It also explores the potential of satellite data integration for RH profile retrieval for the first time. However, there are still problems with individual data at certain times during the fusing process. For example, there are few effective data filtered by quality control methods for FY4B data. Therefore, the matching accuracy and more high-quality FY4B data will be improved in future development.

Declaration of Competing Interest

The authors declare that they have no known competing financial interests or personal relationships that could have appeared to influence the work reported in this paper.

Data availability

Raman lidar, MVR, satellite, radiosonde and other auxiliary data used to generate the results of this paper are available from the authors upon request (email: zychen@btbu.edu.cn).

Acknowledgments

This work was supported by the Innovation and Development Special Project of China Meteorological Administration (No. CXFZ2024J011 and CXFZ2024J057) and National Key Research and Development Program of China (No. 2024YFC3711701) . The authors thank the colleagues who participated in the operation of the lidar system at our site. We also acknowledge the CMA for the satellite (FY4B) data, radiosonde data (https://ladsweb.modaps.eosd is.nasa.gov), and the European Center for Medium – Range Weather Forecasts (ECMWF) for the ERA5 reanalysis data (https://climate.copernicus.eu /climate – reanalysis).

https://doi.org/10.5194/egusphere-2025-1171
Preprint. Discussion started: 19 March 2025

References

Adam, M., Demoz, B.B., Whiteman, D. N., Venable, D.D., Joseph, E., Gambacorta, A., Wei, J., Shephard, M.W., Milosevich, L. M., Barnet, C. D., Herman, R. L., Fitzgibbon, J., and Connell, R.: Water Vapor Measurements by Howard University Raman lidar during the WAVES 2006 Campaign, J. Atmos. Ocean. Tech., 27, 42-60, https://doi.org/10.1175/2009JTECHA1331.1, 2010.

Bai, W., Zhang, P., Liu, H., Zhang, W., Qi, C., Ma, G., and Li, G.: A fast piecewise-defined neural network method to retrieve temperature and humidity profile for the vertical atmospheric sounding system of FengYun-3E satellite. IEEE Trans. Geosci. Remote Sens. 2023, 61, 4100910.

Barrera-Verdejo, M., Crewell, S., Löhnert, U., Orlandi, E., and Di Girolamo, P.: Ground-based lidar and microwave radiometry synergy for high vertical resolution absolute humidity profiling, Atmos. Meas. Tech., 9, 4013-4028, https://doi.org/10.5194/amt-9-4013-2016, 2016.

Blumberg, W.G., Turner, D.D., Löhnert, U., and Castleberry,S.: Ground based temperature and humidity profiling using spectral infrared and microwave observations, Part II: Actual retrieval performance in clear-sky and cloudy conditions, J. Appl. Meteorol., 54, 2305-2319, 2015.

Brocard, E., Jeannet, P., Begert, M., Levrat, G. Philipona, R., Romanens, G. and Scherrer, S.C.: Upper air temperature trends above Switzerland 1959-2011, J. Geophys. Res. Atmos., 118, 4303-4317, doi:10.1002/jgrd.50438, 2013.

Chen, Z.Y., Ji, C. L., Mao, J. J., Wang, Z. C., Jiao, Z. M., Gao, L. N., Xiang, Y. and Zhang, T. S.: Downdraft influences on the differences of PM2.5 concentration: insights from a mega haze evolution in the winter of northern China, Environ. Res. Lett.,19, 014042, 2024.

Cimini, D., Hewison, T., Martin, L., Güldner, J., Gaffard, C., and Marzano, F.: Temperature and humidity profile retrievals from ground-based microwave radiometers during TUC., Meteor. Z., 15, 45-56, doi: https://doi.org/10.1127/0941-2948/2006/0099, 2006.

Crewell and U. Lohnert: Accuracy of boundary layer temperature profiles retrieved with multifrequency multiangle microwave radiometry, IEEE T. Geosic. Remote, 45,7, 2195-2201, doi: 10.1109/TGRS.2006.888434, 2007.

Delanoë, J., and Hogan R. J.: A variational scheme for retrieving ice cloud properties from combined radar, lidar, and infrared radiometer., J. Geophys. Res., 113 (D7): D07204, doi: 10.1029/2007JD009000, 2008.

Fan, J. Zhang, R., Li, G., Tao, W.K., and Li, X.: Effects of aerosols and relative humidity on cumulus clouds, J. Geophys. Res., 112, D14204, https://doi.org/10.1029/2006JD008136, 2007.

Foth, A., Baars, H., Di Girolamo, P., and Pospichal, B.: Water vapor profiles from Raman lidar automatically calibrated by microwave radiometer data during HOPE, Atmos. Chem. Phys., 15, 7753-7763, https://doi.org/10.5194/acp-15-7753-2015, 2015.

Foth, A. and Pospichal, B.: Optimal estimation of water vapour profiles using a combination of Raman lidar and microwave radiometer, Atmos. Meas. Tech., 10, 3325-3344, https://doi.org/10.5194/amt-10-3325-2017, 2017.

Furumoto, J., Kurimoto, K. and Tsuda, T.: Continuous observations of humidity profiles with the Mu Radar-RASS combined with GPS and radiosonde measurements., J. Atmos. Oceanic. Technol., 20, 23-41, 2003.

Granados-Muñoz, M. J., Navas-Guzmán, F., Bravo-Aranda, J. A., Guerrero-Rascado, J.L., Lyamani, H., Valenzuela, A., Titos, G., Fernández-Gálvez, J., and Alados-Arboledas, L.: Hygroscopic growth of atmospheric aerosol particles based on active remote sensing and radiosounding measurements: selected cases in southeastern Spain, Atmos. Meas. Tech., 8, 705-718, https://doi.org/10.5194/amt-8-705-2015, 2015.

Hogg, D., Decker, M., Guiraud, F., Earnshaw, K., Merritt, D., Moran, K., Sweezy, W., Strauch, R., Westwater, E., and Little, G.: An automatic profiler of the temperature, wind and humidity in the troposphere, J. Appl. Meteorol., 22, 807-831, 1983.

Long, L., He, L., Li, J. B., Zhang, W. L. and Zhang, Y.X.: Climatic characteristics of mesoscale convective systems in the warm season in North China. Meteorol. Atmos, Phys., 135, 21, https://doi.org/10.1007/s00703-023-00958-1, 2023.

Kang, Y.Z., Peng, X.D., Wang, S.G., Hu,Y.L., Shang, K.Z.,and Lu, S.: Observational analyses of topographic effects on convective systems in an extreme rainfall event in Northern China, Atmos., Res., 229,127-144,2019.

Madonna, F., Amodeo, A., Boselli, A., Cornacchia, C., Cuomo, V., D'Amico, G., Giunta, A., Mona, L.,and Pappalardo, G.: CIAO: the CNR-IMAA advanced observatory for atmospheric research, Atmos. Meas. Tech., 4, 1191-1208, doi:10.5194/amt- 4-1191-2011, 2011.

Mattis, I., Ansmann, A., Althausen, D., Jaenisch,V.,Wandinger, U., Müller, D., Arshinov, Y.F., Bobrovnikov, S.M., and Serikov, I.B.: Relative-humidity profiling in the troposphere with a Raman lidar., Appl. Opt., 41, 6451-6462, doi:10.1364/AO.41.006451, 2002.

Mochida, M.: Simultaneous measurements of hygroscopic property and cloud condensation nucleus activity of aerosol particles of marine biogenic origin, Western Pacific Air-Sea

https://doi.org/10.5194/egusphere-2025-1171
Preprint. Discussion started: 19 March 2025

Interaction Study, 71-81, America, American Geophysical Union, https://doi.org/10.5047/w-pass.a01.008, 2014.

Navas-Guzmán, F., Fernández-Gálvez, J. Granados-Muñoz, M.J., Guerrero-Rascado, J. L., Bravo-Aranda,J. A., and Alados-Arboledas, L.: Tropospheric water vapour and relative humidity profiles from lidar and microwave radiometry,Atmos. Meas. Tech., 7, 1201-1211, 2014.

Petters, M.D. and Kreidenweis, S.M.: A single parameter representation of hygroscopic growth and cloud condensation nucleus activity, Atmos. Chem. Phys., 7, 1961-1971, https://doi.org/10.5194/acp-7-1961-2007, 2007.

Reichardt, J., Wandinger,U., Klein, V., Mattis,I., Hilber, B., and Begbie, R.: RAMSES: German meteorological service autonomous Raman lidar for water vapor, temperature, aerosol, and cloud measurements, Appl. Opt. 51, 8111-8131, https://doi.org/10.1364/AO.51.008111, 2012.

Schmetz, J.: Good things need time: Progress with the first hyperspectral sounder in geostationary orbit, Geophys. Res. Lett.,48, e2021GL096207, 2021.

Stankov, B.B., Martner, B.E., and Politovich, M.K.: Moisture profiling of the cloudy winter atmosphere using combined remote sensors, J. Atmos. Ocean. Technol., 12 , 488-510, 1995.

Skou, N., Søbjærg, S.S. and Kristensen, S.S.: Future high-performance spaceborne microwave radiometer systems, IEEE Geoscience and Remote Sensing Letters, 19, 1-5, doi: 10.1109/LGRS.2021.3118082, 2022.

Wang, S.F., Lu, F., and Feng.Y.T.: An Investigation of the Fengyun-4A/B GIIRS performance on temperature and humidity retrievals., Atmos. ,13, 1830, 2022.

Toporov, M., and U. Löhnert: Synergy of satellite- and ground-based observations for continuous monitoring of atmospheric stability, liquid water path, and integrated water vapor: theoretical evaluations using reanalysis and neural networks, J. Appl. Meteor. Climatol., 59, 1153-1170, https://doi.org/10.1175/JAMC-D-19-0169.1, 2020

Turner, D.D. and Löhnert, U.: Ground-based temperature and humidity profiling: combining active and passive remote sensors, Atmos. Meas. Tech., 14, 3033-3048, https://doi.org/10.5194/amt-14-3033-2021, 2021.

Wex, H., Stratmann, F., Hennig,T., Hartmann,S., Niedermeier, D., Nilsson, E., Ocskay, R., Rose, D., Salma, I., and Ziese, M.: Connecting hygroscopic growth at high humidities to cloud activation for different particle types, Environ. Res. Lett., 3, 035004, 1-10, 2008.

Ware, R., Carpenter, R., Guldner, J., Liljegren, J., Nehrkorn, T., Solheim, F., and Vandenberghe, F.A.: Multi-channel radiometric profiles of temperature, humidity and cloud liquid, radio Sci., 38, 8079-8032, 2003.

Wang, Z.Z., Wang, W.Y., Tong, X.L., Zhang, Z., Liu, J.Y., Lu, H.H., Ding, J., Wu,Y.T.: Progress in spaceborne passive microwave remote sensing technology and its application (in Chinese)., Chin. J. Space. Sci., 43(6): 986-1015, doi: 10.11728/cjss2023.06.yg15, 2023.

Whiteman, D.N., Melfi, S.H., and Ferrare, R.A.: Raman lidar system for the measurement of water vapor and aerosols in the earth's atmosphere, Appl. Optics, 31, 3068-3082, https://doi.org/10.1364/AO.31.003068, 1992.

Xu, G. R., B. K., Zhang, W.G., Cui, C.G., Dong, X.Q., Liu, Y.Y. and Yan, G.P.: Comparison of atmospheric profiles between microwave radiometer retrievals and radiosonde soundings., J. Geophys. Res. Atmos., 120, 10, 313-10,323, doi: https://doi.org/10.1002/2015JD023438, 2015.

Yang, J., Zhang, Z., Wei, C., Lu, F., and Guo, Q.: Introducing the new generation of Chinese geostationary weather satellites, Fengyun-4. Bull., Am. Meteorol. Soc. 98, 1637-1658, 2017.

Yang, W., Chen, Y., Bai, W., Sun, X., Zheng, H., and Qin, L.: Evaluation of temperature and humidity profiles retrieved from Fengyun-4B and implications for typhoon assimilation and forecasting, Remote Sens. 15, 5339. https://doi.org/10.3390/rs15225339, 2023.

Yang, J. B., Chen, K., Xu, G. R., Gui, L. Q., Lang, L., Zhang, M.Y., Jin, F., Zhang, R. M., and Sun, C.Y.: Research on neural network training retrieval based on microwave radiometer observed brightness temperature data set, Torrential Rain Disaster (in Chinese), 41, 477-487, https://doi.org/10.3969/j.issn.1004-9045.2022.04.012, 2022.

Zhang, L., Liu, M., He, W., Xia, X.G.,Yu, H.N., Li, S., X., and Li, J.: Ground passive microwave remote sensing of atmospheric profiles using WRF simulations and machine learning techniques., J. Meteorol. Res. 38, 680-692 https://doi.org/10.1007/s13351-024-4004-2, 2024.

Zhang, Z., Dong, X. and Zhu, D.: Optimal channel selection of spaceborne microwave radiometer for surface pressure retrieval over Oceans., J. Atmos. Oceanic Technol., 39, 1857-1868, https://doi.org/10.1175/JTECH-D-21-0121.1, 2022.

Zieger, P., Fierz-Schmidhauser, R., Weingartner, E., and Baltensperger, U.: Effects of relative humidity on aerosol light scattering: results from different European sites, Atmos. Chem. Phys., 13, 10609-10631, https://doi.org/10.5194/acp-13-10609- 2013, 2013.

https://doi.org/10.5194/egusphere-2025-1171
Preprint. Discussion started: 19 March 2025

List of Tables

Table 1 Instruments and monitoring parameters

Instrument	Parameters/units	Temporal-spatial Resolution
Raman lidar	Relative humidity (RH)	7.5 m, 3 minutes
Microwave radiometer (MVR)	Temperature (^{O}C), Relative humidity (RH)	50 m, 3 minutes
FY4B	Relative humidity (RH)	1 hour

Table 2 Assessment of the accuracy of four RH retrieval results (lidar, MVR, satellite and synergetic algorithm) compared with radiosonde at 47 sites in China.

Comparison with radiosonde	Number of sample	R	MB (%)	MAB (%)	RMSE (%)
lidar	192111	0.91	0.56	6.7	10.67
MVR	192111	0.82	-1.49	10.79	14.31
satellite	192111	0.74	1.08	13.19	17.02
syngenetic algorithm	192111	0.98	0.42	3.24	5.27

Table 3 The same as Table 2 but at three representative sites in China.

	Comparison with radiosonde	Number of sample	R	RMSE (%)
HHHT (northern China)	lidar	5326	0.85	39
	MVR	5326	0.73	38
	satellite	5326	0.76	35
	syngenetic algorithm	5326	0.90	26
YB (middle China)	lidar	8444	0.85	25
	MVR	8444	0.80	27
	satellite	8444	0.81	33
	synergetic algorithm	8444	0.91	20
QY (southern China)	lidar	11097	0.91	20
	MVR	11097	0.84	22
	satellite	11097	0.78	26
	synergetic algorithm	11097	0.93	16

https://doi.org/10.5194/egusphere-2025-1171
Preprint. Discussion started: 19 March 2025

List of figures

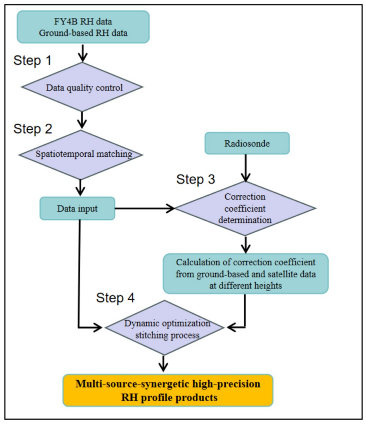

Fig.1 Sketch of the retrieval scheme. Details are given in the text.

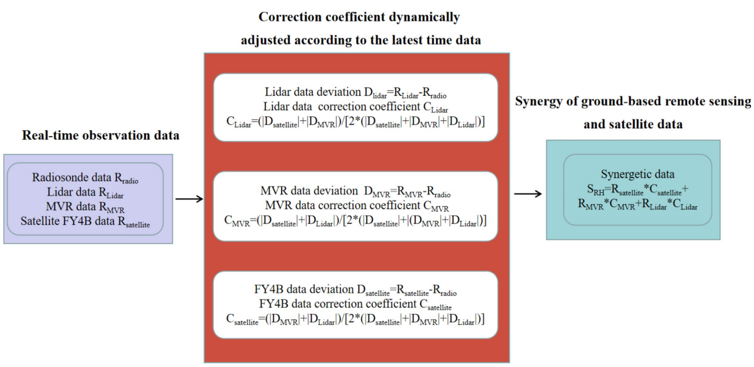

Fig. 2 The dynamic optimal stitching process

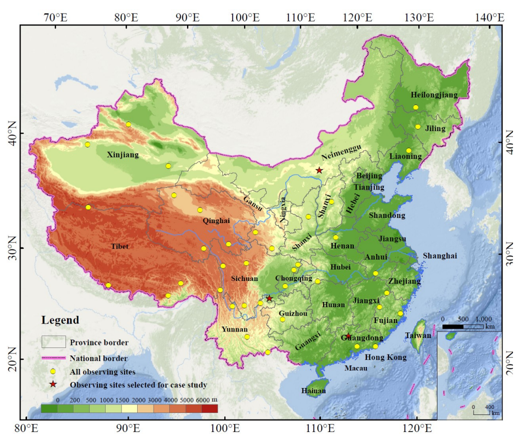

Fig. 3 The observing sites (yellow circles) and three selected sites (red stars) for statistics and case studies are marked in the map.

https://doi.org/10.5194/egusphere-2025-1171
Preprint. Discussion started: 19 March 2025

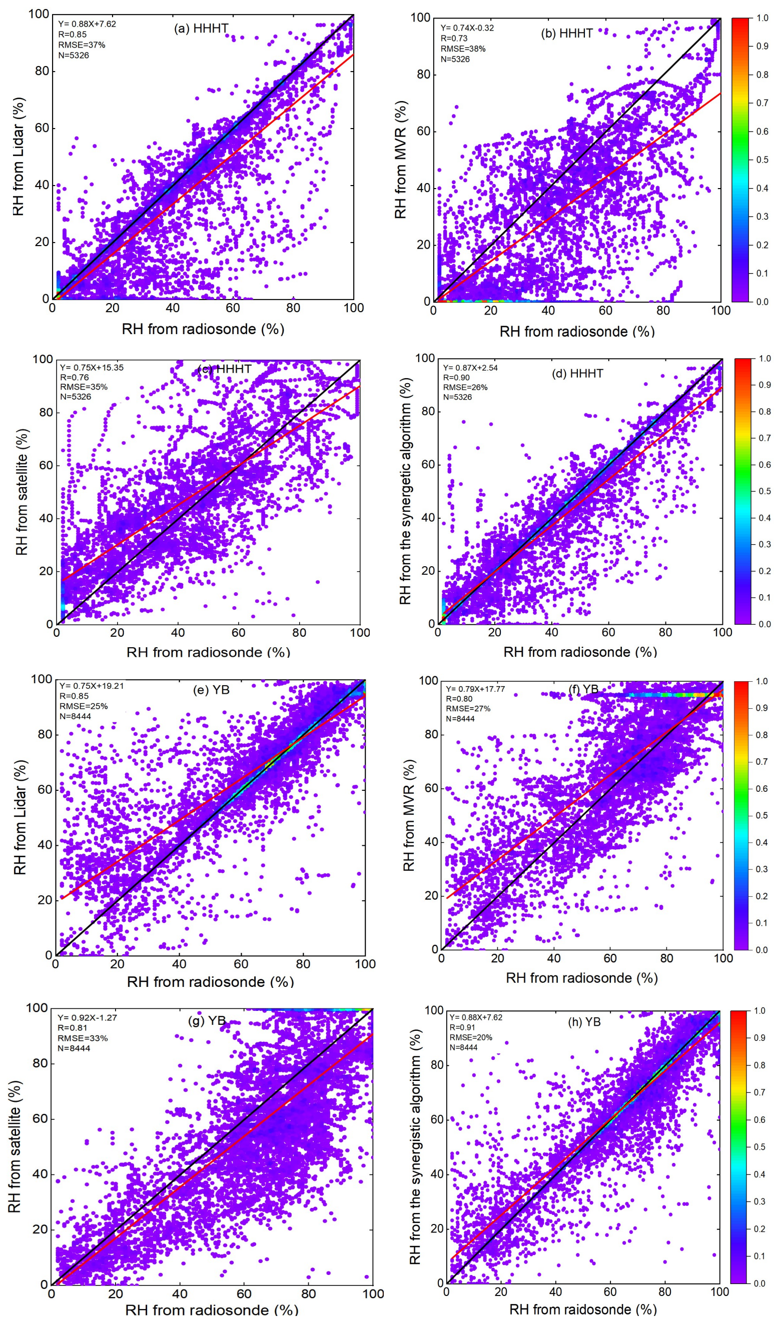

https://doi.org/10.5194/egusphere-2025-1171
Preprint. Discussion started: 19 March 2025

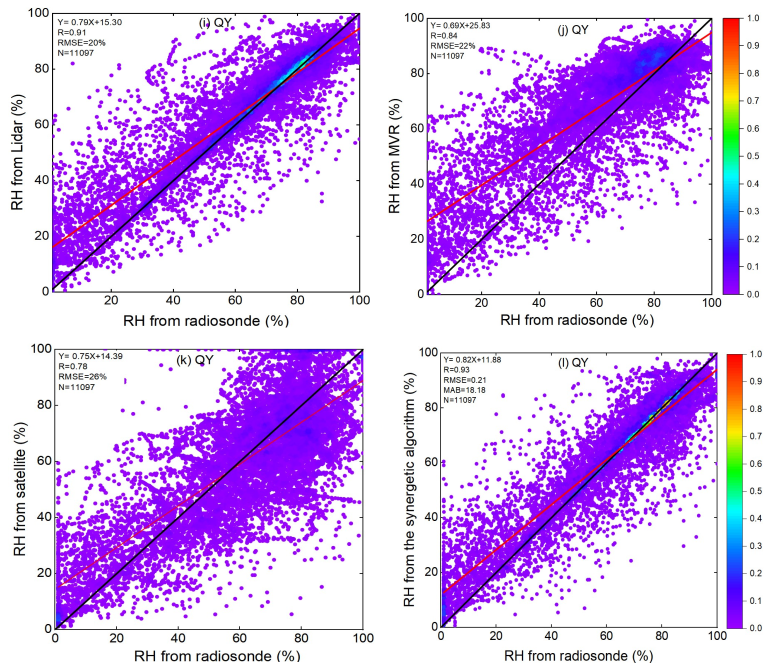

Fig.4 Four-methods-retrieved RH results (lidar, MVR, satellite and synergetic algorithm) compared with radiosonde at three sites in China from 1 July to 31 November 2024. (a) Comparison between lidar and radiosonde in HHHT, (b) Comparison between MVR and radiosonde in HHHT, (c) Comparison between satellite and radiosonde HHHT, (d) Comparison between synergetic algorithm and radiosonde in HHHT; (e)-(h), the same as (a)-(d) but in YB. (i)-(l), the same as (a)-(d) but in QY. The red line shows the regression line. The black line is the one-to-one line.

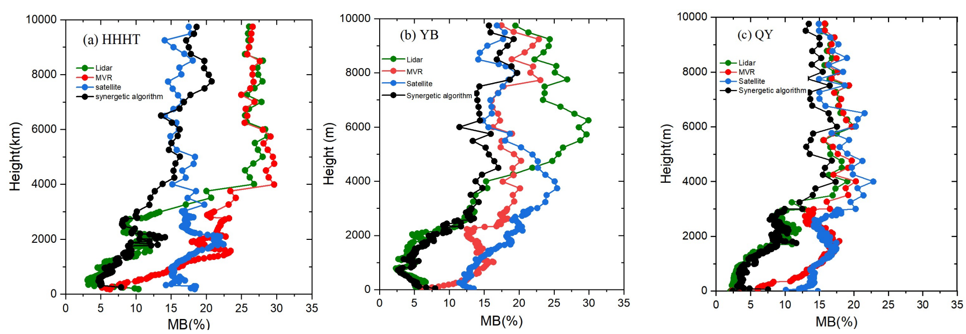

Fig. 5. RH vertical mean bias (MB) profiles retrieved from lidar, MVR, satellite and synergetic algorithm compared to the radiosonde data in (a) HHHT, (b) YB and (c) QY.

https://doi.org/10.5194/egusphere-2025-1171
Preprint. Discussion started: 19 March 2025

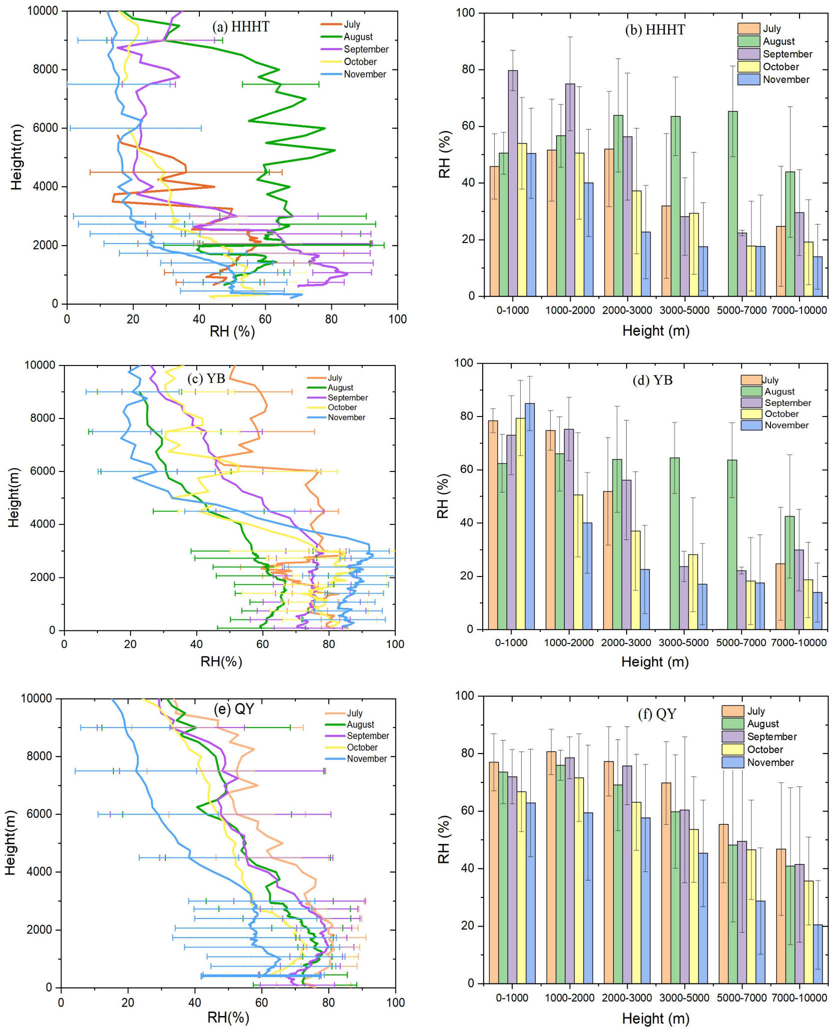

Fig. 6 RH Monthly vertical profiles (left) and monthly mean values for different heights (right) in (a)-(b) HHHT, (c)-(d)YB and (e)-(f) QY. The error bars indicate the standard deviation.

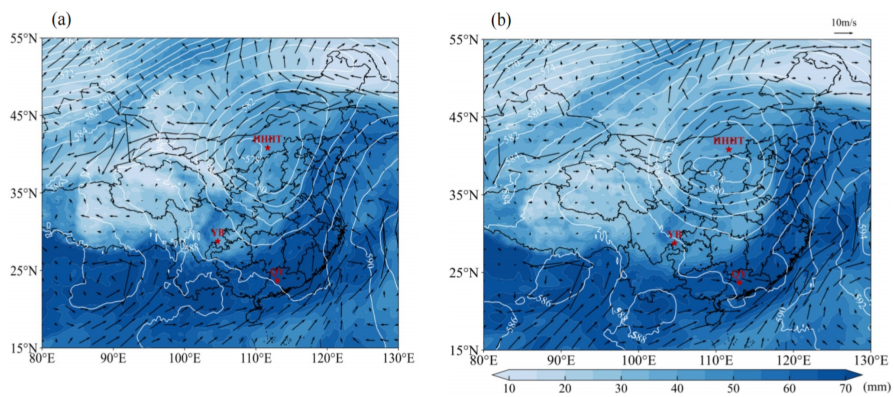

https://doi.org/10.5194/egusphere-2025-1171
Preprint. Discussion started: 19 March 2025

Fig. 7 The ERA5-based 500 hPa (approximately 5500 m) geopotential height field (contour, unit: dagpm), 850 hPa (approximately 1500 m) wind field, and total column precipitable water (shaded) at (a) 20:00 LST August 19, 2024, and (b) 08:00 LST August 20, 2024. HHHT, YB and QY are marked as red stars.

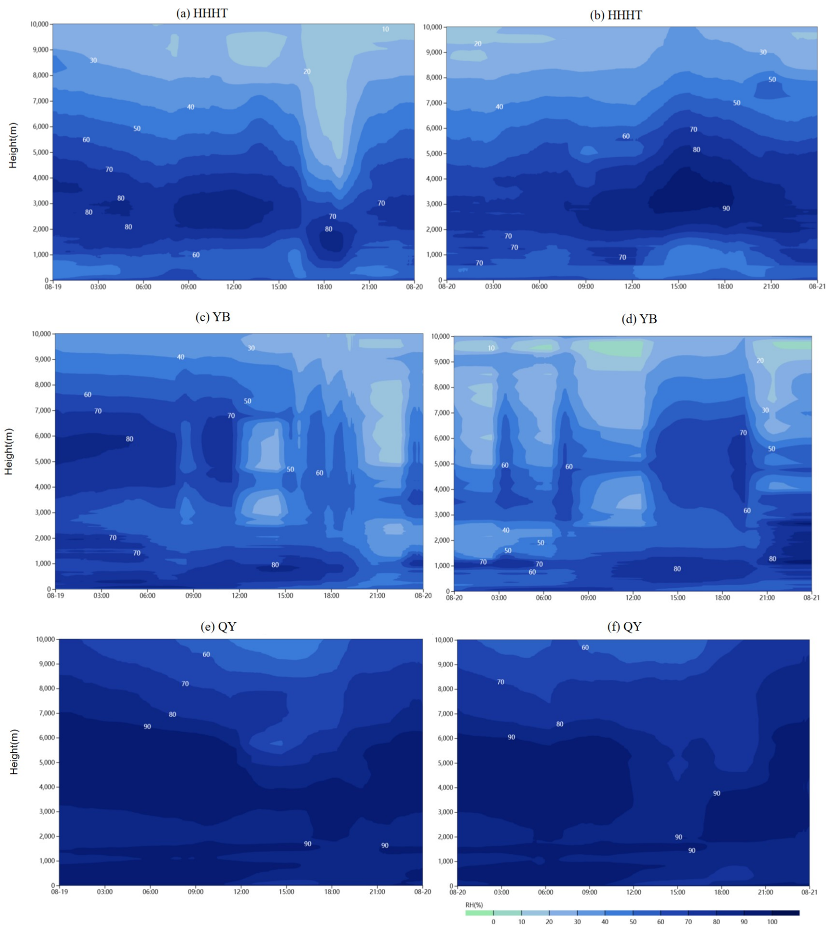

Fig. 8 Height-time display of RH from the synergetic retrieval from 19 to 20 August 2024 LST at (a) - (b) HHHT, (c) - (d) YB and (e) - (f) QY.